Direct detection of WIMPs : Implications of a self-consistent truncated isothermal model of the Milky Way's dark matter halo

Soumini Chaudhury[a*], Pijushpani Bhattacharjee[a†], Ramanath Cowsik[b‡]
[a] *AstroParticle Physics and Cosmology Division & Centre for AstroParticle Physics (CAPP), Saha Institute of Nuclear Physics, 1/AF Bidhannagar, Kolkata 700064. India*
[b] *McDonnell Center for the Space Sciences and Department of Physics, Washington University, St. Louis, MO 63130, USA*

Direct detection of Weakly Interacting Massive Particle (WIMP) candidates of Dark Matter (DM) is studied within the context of a self-consistent truncated isothermal model of the finite-size dark halo of the Galaxy. The halo model, based on the "King model" of the phase space distribution function of collisionless DM particles, takes into account the modifications of the phase-space structure of the halo due to the gravitational influence of the observed visible matter in a self-consistent manner. The parameters of the halo model are determined by a fit to a recently determined circular rotation curve of the Galaxy that extends up to ~ 60 kpc. Unlike in the Standard Halo Model (SHM) customarily used in the analysis of the results of WIMP direct detection experiments, the velocity distribution of the WIMPs in our model is non-Maxwellian with a cut-off at a maximum velocity that is self-consistently determined by the model itself. For our halo model that provides the best fit to the rotation curve data, the 90% C.L. upper limit on the WIMP-nucleon spin-independent cross section from the recent results of the CDMS-II experiment, for example, is $\sim 5.3\times10^{-8}$ pb at a WIMP mass of ~ 71 GeV. We also find, using the original 2-bin annual modulation amplitude data on the nuclear recoil event rate seen in the DAMA experiment, that there exists a range of small WIMP masses, typically $\sim$ 2 – 16 GeV, within which DAMA collaboration's claimed annual modulation signal purportedly due to WIMPs is compatible with the null results of other experiments. These results, based as they are on a self-consistent model of the dark matter halo of the Galaxy, strengthen the possibility of low-mass ($\lesssim 10\,$GeV) WIMPs as a candidate for dark matter as indicated by several earlier studies performed within the context of the SHM. A more rigorous analysis using DAMA bins over smaller intervals should be able to better constrain the "DAMA regions" in the WIMP parameter space within the context of our model.

* soumini.chaudhury@saha.ac.in
† pijush.bhattacharjee@saha.ac.in
‡ cowsik@wuphys.wustl.edu

I. INTRODUCTION

One of the most favored candidates for the Dark Matter (DM), that constitutes roughly a quarter of the mass-energy density of the Universe [1], is some kind of Weakly Interacting Massive Particles (WIMPs) with masses typically between a few GeV and a few TeV. Such particles are predicted in many models of physics beyond the Standard Model of particle physics such as models involving supersymmetry or higher (spatial) dimensional theories [2–4]. Owing to their weak interactions, such particles would "freeze out" in the early Universe at a characteristic temperature scale of $\sim$ MeV, and would be present in the Universe today as 'cold' dark matter with a calculable abundance that can naturally explain the measured average cosmological density of dark matter in the Universe. Also, the measured rotation curves of spiral galaxies, such as that of our own, the Milky Way, out to and beyond their visible edges, can be explained naturally under the hypothesis that the visible galaxies are embedded in much larger, roughly spherical, dark matter "halos". The true extents and the masses of such halos are, however, unknown.

Following early suggestions [5–7] (see [8] for a review), several experiments worldwide are currently engaged in attempts to directly detect these hypothetical WIMP DM particles comprising the DM Halo of the Milky Way (the Galaxy, hereafter) in terrestrial laboratories. These direct detection experiments attempt to detect nuclear recoils resulting from interaction of WIMPs with a suitably chosen target material in underground laboratory detectors with low backgrounds.

The DAMA/NaI [9] and DAMA/LIBRA [10] experiments (hereafter together simply referred to as the "DAMA" collaboration) have reported an annual modulation signal in their event rate at a confidence level of 8.2σ based on their combined data [10]. They interpret this as evidence for WIMPs, ascribing the modulation to the periodic variation of the flux of WIMPs passing through the detector on earth caused by the orbital motion of the earth around the sun. The CDMS-II collaboration [11] has also reported two candidate events in their "signal region" with an estimated probability of $\sim 23\%$ of observing 2 or more background events in that region, for the estimated level of the background. Several other experiments such as CRESST [12], XENON10 [13, 14], COUPP [15] and PICASSO [16], for example, have reported only null results so far. These results provide important constraints on the WIMP mass and WIMP-nucleon interaction cross section. The question of compatibility of the DAMA results [10] with the negative results from other experiments has also been the subject of several recent studies which include the earlier overlooked effect of "ion channeling" (see below) on the analysis of the DAMA results [17–19].

In order to derive constraints on (or to determine) the mass and interaction cross section of the unknown WIMP DM particles from the results of these direct detection experiments, one requires the density and velocity distribution of the WIMPs in the solar neighborhood as crucial input parameters. These parameters are *a priori* unknown. In the customary analysis the DM halo of the Galaxy is assumed to be described by a single component isothermal sphere [20] with a Maxwellian velocity distribution in the Galactic rest frame given by

$$f(\mathbf{x},\mathbf{v})d^3\mathbf{v} = 4\pi\rho(\mathbf{x})\left[\frac{3}{2\pi\langle v^2\rangle}\right]^{\frac{3}{2}} v^2 \exp\left[-\frac{3}{2}\frac{v^2}{\langle v^2\rangle}\right] dv\,. \tag{1}$$

Here $v = |\mathbf{v}|$, $\rho(\mathbf{x})$ is the density at the location $\mathbf{x}$, and $\langle v^2\rangle^{1/2}$ is the velocity dispersion. The justification for this Maxwellian form comes from the work of Lynden-Bell [21] who argued that evolution of systems of collisionless particles (such as WIMPs) under the process of gravitational collapse is governed by the process of "violent relaxation" whereby the observationally relevant 'coarse-grained' phase space distribution function (DF) of the system rapidly relaxes, due to collective effects, to a quasi-Maxwellian stationary state which is a steady-state solution of the collisionless Boltzmann equation.[1]

The DM density in the solar neighborhood is usually taken to be $\rho_{\rm DM,\odot} \sim 0.3 \pm 0.1\,{\rm GeV/\,cm^3}$, following the analysis of the observed velocity distribution of stars transverse to the Galactic disk near the sun, as suggested by Oort [22] and extended by Bahcall [23]. A recent "model-independent" analytical study [24] quotes $\rho_{\rm DM,\odot} = 0.43 \pm 0.11 \pm 0.10\,{\rm GeV/\,cm^3}$. Also, a recent attempt to directly extract this density from the results of cosmological large N-body simulations yields a value of $\rho_{\rm DM,\odot} \sim 0.37\,{\rm GeV\,cm^{-3}}$ [25]. The last Reference also finds a DM particle velocity distribution that can in general be called "quasi-Maxwellian", albeit with significant deviation

[1] The 'fine-grained' DF may, however, never reach equilibrium.

from the pure Maxwellian form especially at the high velocity end where it drops off more sharply compared to the pure Maxwellian.

The value of the velocity dispersion, $\langle v^2\rangle^{1/2}$, the single parameter that characterizes the Maxwellian velocity distribution (1) of the DM particles, is usually determined from the relation [20], $\langle v^2\rangle^{1/2} = \sqrt{\frac{3}{2}} v_{c,\infty}$, between the velocity dispersion of the particles constituting a single-component self-gravitating isothermal sphere and the asymptotic value of the circular rotation speed, $v_{c,\infty}$, of a test particle in the gravitational field of the isothermal sphere. Neglecting the effect of the visible matter on the DM halo, and assuming $v_{c,\infty} \approx v_{c,\odot} \approx 220\,\mathrm{km\,s^{-1}}$, where $v_{c,\odot}$ is the measured value of the circular rotation velocity of the Galaxy in the solar neighborhood, one gets $\langle v^2\rangle^{1/2}{}_{\rm iso} \approx 270\,\mathrm{km\,s^{-1}}$. [2] This isothermal sphere model of the DM halo with a value of the DM velocity dispersion $\langle v^2\rangle^{1/2}_{\rm DM} \simeq 270\,\mathrm{km\,s^{-1}}$ and local value of the DM density $\rho_{\rm DM,\odot} \simeq 0.3\,\mathrm{GeV\,cm^{-1}}$ is what is often referred to as the *Standard Halo Model* (SHM). This SHM is generally taken as a sort of benchmark model of the DM halo of the Galaxy, and the results of various WIMP DM search experiments are mostly analyzed within the context of this SHM.

Whereas the SHM would suffice for the initial design of the experiments, it is necessary to consider improved models to analyze the results of the experiments, which are becoming progressively more sophisticated. The reasons for this are many: (1) It is well-known that the isothermal sphere has a mass that linearly increases with its radius r and tends to ∞ as $r \to \infty$. Clearly, such a system cannot represent a realistic DM halo of finite physical size. (2) The rotational speed in the isothermal sphere model increases linearly for small r, has an oscillatory dependence on r for intermediate r, and tends to a constant only asymptotically as $r \to \infty$. Thus there is no strict reason why $v_{c,\infty}$ should be equal to $v_{c,\odot}$. (3) More importantly, the presence of the visible matter further complicates the situation; it contributes significantly to balancing the centrifugal forces of rotation at the solar circle. The density profile of an isothermal sphere is obtained as the solution to a second-order non-linear differential equation with appropriate boundary conditions at the origin. Thus the presence of a significant amount of visible matter within the solar circle will substantially change the nature of the solutions. (4) It is a common practice, in the context of the phenomenology of DM direct detection experiments, to truncate the speed distribution (1) at some chosen value of the local (solar neighborhood) escape speed $v_{\rm escp}$; see, e.g., [7, 8]). However, this is not in general a self-consistent procedure because the resulting "truncated Maxwellian" speed distribution will not necessarily be a solution of the steady-state collisionless Boltzmann equation appropriate for a finite physical system. In addition, since the rotation curve for such a truncated Maxwellian will not in general be asymptotically flat, the relation $\langle v^2\rangle^{1/2} = \sqrt{\frac{3}{2}} v_{c,\infty}$ used to determine the value of $\langle v^2\rangle^{1/2}$ in the Maxwellian speed distribution of the isothermal sphere, as done in the SHM, will not be valid. However, there are indeed well understood procedures that allow truncation of the DM halo at a finite radius and the velocity distribution at appropriate limits in a self-consistent manner.

In this paper we construct a self-consistent model of the phase-space structure of the finite-size DM halo of the Galaxy, and study its implications for the analysis of the results of the direct detection experiments. The model is based on describing the phase-space DF of the DM particles in the halo by the so-called "lowered" (or truncated) isothermal models (often called "King models") [20], which are proper self-consistent solutions of the collisionless Boltzmann equation representing nearly isothermal systems of finite physical size and mass. At every location $\mathbf{x}$ within the system a DM particle can have speeds up to a maximum speed $v_{\rm max}(\mathbf{x})$, which is self-consistently determined by the model itself. A particle of velocity $v_{\rm max}(\mathbf{x})$ at $\mathbf{x}$ within the system can just reach its outer boundary, generally called the truncation radius, where the DM density by construction vanishes. Note that this maximum speed $v_{\rm max}$ is not the same as the escape speed $v_{\rm escp}$, which is defined as the speed required for a particle to escape from the given location out to infinity. The escape speed is always larger than the maximum speed. For a King model DM halo of finite size, it is the maximum speed and not the escape speed that is relevant in considerations of direct detection experiments. As we shall see below, the speed distribution of the particles constituting a lowered isothermal model can be described as "quasi-Maxwellian" not unlike what is seen in recent simulations [25]. Apart from taking into account the finite size of the DM halo, we also explicitly account for the mutual gravitational interaction between the visible matter and the DM, as this interaction influences both the density profile and the velocity distribution of the dark matter particles. When the visible matter density is set to zero and the truncation radius is set to infinity, our halo model becomes identical to that of a single-component isothermal sphere used in the SHM.

---

[2] A recent study suggests a somewhat higher value of $v_{c,\odot} \approx 250\,\mathrm{km\,s^{-1}}$ [26], which would imply a correspondingly higher value of $\langle v^2\rangle^{1/2}{}_{\rm iso} \approx 306\,\mathrm{km\,s^{-1}}$.

The model we develop here is along the lines described in earlier formulations [27, 28] which included the effects of the gravitation of the visible matter on the dark matter in a self-consistent manner. Stated simply, these models account for the fact that the DM particles move in a gravitational potential to which both the visible matter and the dark matter make contributions. As the distribution of the visible matter may be fixed from observations, the parameters of the self-consistent velocity distribution function of the DM particles in presence of the visible matter can be determined by comparing the theoretically derived rotation curve with the observed rotation curve of the Galaxy. The velocity distribution function so determined is then used in the calculation of the direct detection rates.

Of particular interest in this context is the rotation curve recently reported by Xue et al [29], which extends up to a galactocentric distance of $\sim 60\,\mathrm{kpc}$. This rotation curve is derived from the kinematics of a sample of ~ 2400 blue horizontal-branch (BHB) stars taken from the Sloan Digital Sky Survey (SDSS) DR6 [30] database. A noticeable feature of this rotation curve is that it gently falls from the adopted value at the Sun's location, $v_{c,\odot} \approx 220\,\mathrm{km\,s^{-1}}$, to $\sim 180\,\mathrm{km\,s^{-1}}$ at $\sim 60\,\mathrm{kpc}$. It is of considerable interest to study the implications of such a rotation curve for the direct detection experiments. In this paper, therefore, we use this new rotation curve for determining the parameters of our halo model.

For the isothermal sphere model of the DM halo, the main effect of the gravitational influence of the visible matter on the structure of the DM halo is to shrink its 'core radius' [20], $r_0 \equiv \left(3\langle v^2\rangle/(4\pi G\rho_0)\right)^{1/2}$, where ρ_0 is the central density [3]. This is because the DM is "pulled in" by the visible matter, increasing its effective central density. Thus the characteristic core radius of an isothermal DM distribution in presence of the visible matter is less than that of an isolated isothermal sphere whose properties are determined by its own gravity alone. The same, as we show below, is true for the lowered isothermal models. A related effect is the relative enhancement of the DM density near the plane of the disk due to additional gravitational influence of the disk. These effects are further discussed in the following section.

We find that, for our best-fit halo model with parameter values $\rho_{\mathrm{DM},\odot} = 0.2\,\mathrm{GeV/\,cm^3}$ and truncation radius $r_t = 120\,\mathrm{kpc}$, that provides the best fit to the rotation curve data of Ref. [29], the null result of the CDMS-II experiment [11], for example, gives a 90% C.L. upper limit on the WIMP-nucleon spin-independent (SI) cross section of $\sim 5.3\times10^{-8}\,\mathrm{pb}$ for a WIMP mass of ~ 71 GeV.

We also study the issue of compatability of the claimed positive signal reported by the DAMA collaboration with the null results from the other experiments using, for illustration, the DAMA collaboration's original 2-bin annual modulation amplitude data. We find that for our best-fit halo model, there exists a region of the WIMP mass (m_χ) vs. WIMP-nucleon spin-independent (SI) cross section ($\sigma^{\mathrm{SI}}_{\chi p} = \sigma^{\mathrm{SI}}_{\chi n}$) parameter space bounded by $2.6 \lesssim m_\chi \lesssim 10.8\,\mathrm{GeV}$ and $1.0\times10^{-2} \gtrsim \sigma^{\mathrm{SI}}_{\chi p} \gtrsim 1.2\times10^{-5}\,\mathrm{pb}$, within which the DAMA's claimed modulation signal is compatible with the null results of other experiments. Similar "DAMA-compatible" regions of small WIMP masses obtain also for spin-dependent interactions. We, however, recognize that a more rigorous analysis using DAMA bins over smaller intervals should be able to better constrain the DAMA region within the context of our halo model, a task that we will take up in a subsequent work.

The rest of the paper is arranged as follows: In section II we describe our model of the dark halo of the Galaxy that includes in a self-consistent manner the gravitational effect of the observed visible matter on the structure of dark matter halo. The parameters of the model are determined by fitting the theoretically calculated rotation curves to a recently determined extended rotation curve of the Galaxy up to $\sim 60\,\mathrm{kpc}$. The shapes of the dark matter density and mass profiles and the velocity distribution function of the DM particles are also derived. The implications of our model for the analysis of the results of WIMP direct detection experiments including the question of compatibility of DAMA's claimed positive signal with the null results of other experiments, are studied in section III. Section IV

[3] The gravitational effect of the Galactic disk, of course, flattens the isothermal 'sphere'. Our formalism in this paper automatically and self-consistently incorporates this effect. Below, unless otherwise specified, by core radius we refer to that of the density distribution in the plane of the Galactic disk. Note, however, that while the resulting density distribution of the halo becomes anisotropic, one can still assume, as we do in this paper, that the velocity distribution of the DM particles remains isotropic everywhere, although anisotropic (velocity) models are also possible [20]. The effects of anisotropic and also triaxial halo models on the event rates in direct detection experiments and the resulting nature of the exclusion limits on WIMP parameters have been studied earlier; see, e.g., Ref. [31] and references therein.

summarizes the main results of this paper and concludes.

In this paper we restrict our attention to only elastic scattering of WIMPs from nuclei due to spin-independent (SI) as well as spin-dependent (SD) WIMP-nucleus interactions.

II. THE SELF-CONSISTENT TRUNCATED ISOTHERMAL MODEL OF THE DARK MATTER HALO OF THE GALAXY

A. The Basic Formalism

The Maxwellian velocity distribution (1) used in the SHM is simply related to the phase-space DF of the isothermal sphere [20],

$$f_{\rm IS}(\mathbf{x},\mathbf{v}) = f(E) = \frac{\rho_0}{(2\pi\sigma^2)^{\frac{3}{2}}} \exp\left[-E/\sigma^2\right] \,, \tag{2}$$

with $\langle v^2 \rangle = 3\sigma^2$ and $E = \Phi(\mathbf{x}) + \frac{1}{2}v^2$, the total energy (per unit mass) of the DM particle, $\Phi(\mathbf{x})$ being the total gravitational potential with the boundary condition $\Phi(0) = 0$, so that the density at any point $\mathbf{x}$ is

$$\rho_{\rm IS}(\mathbf{x}) = \int f_{\rm IS}(\mathbf{x},\mathbf{v}) d^3\mathbf{v} = \rho_0 \exp\left[-\Phi(\mathbf{x})/\sigma^2\right] \,, \tag{3}$$

where ρ_0 is the central density. The isothermal sphere described by DF (2) is infinite in extent with a divergent total mass, and is characterized by two parameters, σ and ρ_0.

To describe "nearly isothermal" systems of finite size and finite total mass, one must have, in addition to the above two parameters of the isothermal sphere, a parameter that characterizes the finite size of the system. This is accomplished in King models by taking the DF to be of the following form [20]:

$$f_{\rm K}(\mathbf{x},\mathbf{v}) \equiv f(\mathcal{E}) = \begin{cases} \rho_1 (2\pi\sigma^2)^{-3/2} \left(e^{\mathcal{E}/\sigma^2} - 1\right) & \text{for } \mathcal{E} > 0 \,, \\ 0 & \text{for } \mathcal{E} \leq 0 \,, \end{cases} \tag{4}$$

where

$$\mathcal{E}(\mathbf{x}) \equiv \mathcal{C} - \left(\frac{1}{2}v^2 + \Phi(\mathbf{x})\right) \equiv \Psi(\mathbf{x}) - \frac{1}{2}v^2 \,, \tag{5}$$

is the so-called "relative energy" and $\Psi(\mathbf{x})\,(\equiv -\Phi(\mathbf{x}) + \mathcal{C})$ the "relative potential" [20]. The three (constant) parameters of the system are ρ_1 (with dimension of density), σ (with dimension of velocity) and the new parameter $\mathcal{C}$ (with dimension of potential or squared velocity) which is related to the finite size of the system (see below).

The density at any position $\mathbf{x}$ is obtained by integrating $f_{\rm K}(\mathbf{x},\mathbf{v})$ over all velocities giving

$$\rho_{\rm K}(\mathbf{x}) = \frac{\rho_1}{(2\pi\sigma^2)^{3/2}} \int_0^{\sqrt{2\Psi(\mathbf{x})}} dv\, 4\pi v^2 \left[\exp\left(\frac{\Psi(\mathbf{x}) - v^2/2}{\sigma^2}\right) - 1\right] \tag{6}$$

$$= \rho_1 \left[\exp\left(\frac{\Psi(\mathbf{x})}{\sigma^2}\right) \,{\rm erf}\left(\frac{\sqrt{\Psi(\mathbf{x})}}{\sigma}\right) - \sqrt{\frac{4\Psi(\mathbf{x})}{\pi\sigma^2}} \left(1 + \frac{2\Psi(\mathbf{x})}{3\sigma^2}\right)\right] \,, \tag{7}$$

which satisfies the Poisson equation

$$\nabla^2\Phi(\mathbf{x}) = -\nabla^2\Psi(\mathbf{x}) = 4\pi G \rho_{\rm K}(\mathbf{x}) \,. \tag{8}$$

At any location $\mathbf{x}$ the maximum speed a particle of the system can have is

$$v_{\rm max}(\mathbf{x}) = \sqrt{2\Psi(\mathbf{x})} \,, \tag{9}$$

at which the relative energy $\mathcal{E}$ and, as a consequence, the DF (4), vanish.

The King models approach the isothermal sphere solution at small radii $r = |\mathbf{x}|$, but have density profiles that fall off faster than that of the isothermal sphere at large radii (which makes the total mass finite). Indeed, the density vanishes at $r = r_t$, the truncation radius where $\mathcal{E} = 0$, representing the outer edge of the system. This is ensured by choosing

$$\mathcal{C} = \Phi(r_t)\,, \quad \text{so that } \Psi(r_t) = -\Phi(r_t) + \mathcal{C} = 0\,. \tag{10}$$

As evident from Equation (10), the parameter $\mathcal{C}$ fixes the finite size (r_t) of the system. Actually, the King models form a sequence, each model being parametrized by the value of the "concentration parameter" C/σ^2. It can be shown [20] that the sequence of King models goes over into the isothermal sphere in the limit $C/\sigma^2 \to \infty$.

Note that the usual escape speed, $v_{\rm escp}$, defined as $v^2_{\rm escp}(\mathbf{x}) = 2\,[\Phi(\infty) - \Phi(\mathbf{x})]$ is related to the maximum speed $v_{\rm max}(\mathbf{x})$ defined by equation (9) through the relation

$$\begin{aligned} v^2_{\rm max}(\mathbf{x}) \; &= 2\Psi(\mathbf{x}) = 2\,[\Phi(r_t) - \Phi(\mathbf{x})] \\ &= v^2_{\rm escp}(\mathbf{x}) - 2\,{\rm G}M(r_t)/r_t\,, \end{aligned} \tag{11}$$

where $M(r_t)$ is the mass contained within r_t, with[4] ${\rm G}M(r_t)/r_t = [\Phi(\infty) - \Phi(r_t)]$. Note also that, unlike in the case of the (infinite) isothermal sphere, the parameter σ in the King models is *not* equal to the one-dimensional velocity dispersion of the particles constituting the system; the latter can be calculated for the DF given above and is a function of r, vanishing at $r = r_t$. In fact, unlike in the case of the Maxwellian DF for which the velocity dispersion is linearly related to the most probable speed of the particles of the system, there is no simple relation between the velocity dispersion and the most probable speed of the particles of the system described by a skewed velocity distribution such as that described by the King DF (4), and as such, the velocity dispersion has no special significance and does not uniquely specify the full DF of the King model.

In the subsequent discussions we shall take the King model DF (4) as the DF of the DM particles constituting the finite-size DM halo of the Galaxy, *in the rest frame of the Galaxy* (the subscript K will be dropped for convenience).

For a "pure" DM halo of finite size represented by the DF (4) without including the gravitational influence of the visible matter embedded within the halo, the gravitational potential Φ in the above equations can be written as $\Phi(\mathbf{x}) = \Phi^{(0)}_{\rm DM}(r)$, where $\Phi^{(0)}_{\rm DM}(r)$ is the spherically symmetric self-gravitational potential of the pure DM halo represented by the DF (4). In reality, however, a test particle sees the total gravitational potential of both the DM and the visible matter embedded within the DM halo. Thus, we should write

$$\Phi(\mathbf{x}) = \Phi_{\rm DM}(\mathbf{x}) + \Phi_{\rm vis}(\mathbf{x})\,, \tag{12}$$

where now $\Phi_{\rm DM}$ represents the contribution of the DM component to the total gravitational potential *in presence of the visible matter*, and $\Phi_{\rm vis}$ is the gravitational potential of the observed visible matter of the Galaxy. These potentials satisfy their respective Poisson equations

$$\nabla^2\Phi_{\rm DM}(\mathbf{x}) = 4\pi G\rho_{\rm DM}(\mathbf{x})\,, \quad \text{and } \; \nabla^2\Phi_{\rm vis}(\mathbf{x}) = 4\pi G\rho_{\rm vis}(\mathbf{x})\,, \tag{13}$$

where the DM density is

$$\rho_{\rm DM}(\mathbf{x}) = \rho_1 \left[\exp\left(\frac{\Psi(\mathbf{x})}{\sigma^2}\right)\,{\rm erf}\left(\frac{\sqrt{\Psi(\mathbf{x})}}{\sigma}\right) - \sqrt{\frac{4\Psi(\mathbf{x})}{\pi\sigma^2}}\left(1 + \frac{2\Psi(\mathbf{x})}{3\sigma^2}\right)\right]\,, \tag{14}$$

with

$$\Psi(\mathbf{x}) = \Big[\Phi_{\rm DM}(|\mathbf{x}| = r_t) + \Phi_{\rm vis}(|\mathbf{x}| = r_t)\Big] - \Big[\Phi_{\rm DM}(\mathbf{x}) + \Phi_{\rm vis}(\mathbf{x})\Big]\,, \tag{15}$$

---

[4] Note that we have chosen the boundary condition $\Phi(0) = 0$, so that $\Phi(\infty)$ is a non-zero positive constant.

using (10), and $\rho_{\rm vis}$ is the known visible matter density of the Galaxy.

Note that in presence of the visible matter, whose spatial distribution is non-spherically symmetric, the DM spatial distribution and hence its gravitational potential will also be non-spherically symmetric in general. However, for large enough values of the truncation radius (r_t) of the halo (more specifically, for r_t large compared to the visible matter disk's scale length — the latter being $\sim$ few kpc; see below), both $\Phi_{\rm DM}$ and $\Phi_{\rm vis}$ become close to spherically symmetric at $|\mathbf{x}| \to r_t$, which we also see in our numerical calculations described below. On the other hand, as already mentioned in footnote 3 in Section I, the velocity distribution will be assumed to remain isotropic.

The visible matter distribution $\rho_{\rm vis}(\mathbf{x})$ (and hence the potential $\Phi_{\rm vis}(\mathbf{x})$) being known from various observational data and modeling, solutions of equations (13), (14), (15) with appropriate boundary conditions, which we choose as

$$\Phi_{\rm DM}(0) = \Phi_{\rm vis}(0) = 0\,, \quad \text{and} \quad (\nabla\Phi_{\rm DM})_{|\mathbf{x}|=0} = (\nabla\Phi_{\rm vis})_{|\mathbf{x}|=0} = 0\,, \tag{16}$$

give us a three-parameter family of self-consistent solutions for $\rho_{\rm DM}(\mathbf{x})$ and $\Phi_{\rm DM}(\mathbf{x})$ for chosen values of the parameters $(\rho_1\,, \sigma\,, r_t)$.

For a given solution, the rotation curve of the Galaxy, $v_c(R)$, i.e., the circular rotation velocities in the equatorial plane of the Galaxy as a function of the Galactocentric distance (R) on the equatorial plane, can be calculated from

$$v_c^2(R) = R\frac{\partial}{\partial R}\Big[\Phi_{\rm total}(R, z=0)\Big] = R\frac{\partial}{\partial R}\Big[\Phi_{\rm DM}(R, z=0) + \Phi_{\rm vis}(R, z=0)\Big]\,, \tag{17}$$

z being the distance normal to the equatorial plane. The best-fit values of the relevant parameters can then be determined by comparing the theoretically calculated rotation curves with the observed data on the rotation curve of the Galaxy. The parameter values so determined are then to be used as inputs to the analysis of the results of the direct detection experiments.

We have developed an efficient numerical scheme to solve the coupled non-linear Poisson equation (13) for DM with $\rho_{\rm DM}$ given by equations (14) and (15) with boundary conditions (16), for a given potential–density pair of the visible matter, through an iterative procedure first discussed in [27]. Each stage of this iteration procedure involves a Poisson solver which is tested on a number of exact analytical formulae for potential–density pairs given, for example, in [20]. The iteration process converges typically within ten iterations. We have also verified that this iterative scheme yields good agreement with the known results for both the non-singular isothermal sphere and King Models given in [20], to within a few percent.

We assume that the density distribution of the visible matter can be effectively described by the well-known model of a spheroidal bulge superposed on an axisymmetric disk [32]. The density distributions of these components are given, respectively, by

$$\rho_s(r) = \rho_s(0)\left(1 + \frac{r^2}{a^2}\right)^{-3/2}\,, \tag{18}$$

and

$$\rho_d(r) = \frac{\Sigma_\odot}{2h} e^{-(R-R_0)/R_d}\;\; e^{-|z|/h}\,, \tag{19}$$

where $r = (R^2 + z^2)^{1/2}$. Typical parameter values are [32, 33] $\rho_s(0) = 4.2\times10^2\, M_\odot\,{\rm pc}^{-3}$, $a = 0.103\,{\rm kpc}$, $R_d = 3\,{\rm kpc}$, and $h = 0.3\,{\rm kpc}$, with $R_0 = 8.5\,{\rm kpc}$, the solar Galactocentric distance, and $\Sigma_\odot \approx 48\, M_\odot\,{\rm pc}^{-2}$, the surface density of the disk at the solar location. The expressions for the gravitational potentials, ϕ_s and ϕ_d, corresponding to above forms of ρ_s and ρ_d, are given in [32]. Alternatively, they can be directly calculated using our numerical Poisson solver. This specifies the $\Phi_{\rm vis} = \phi_s + \phi_d$ used in the numerical calculations in this paper.

There exist more detailed models of the mass distribution of the visible matter in the Galaxy than those adopted above, involving a stellar "thick disk" (with a scale height of $\sim 1\,{\rm kpc}$) and the disk formed by the Galaxy's interstellar medium (ISM) in addition to the stellar spheroid and the "thin" disk described by equations (18) and (19). However, there are also large uncertainties in the values of the parameters that characterize these various components, as clear

from the values of the parameters of the two representative models summarized, for example, in Table 2.3 of Ref. [20]. We find, as shown below, that the typical values of the various visible matter parameters chosen above give reasonably good fit to the rotation curve data in the inner Galaxy region, $R \lesssim R_\odot \approx 8.5\,\mathrm{kpc}$, where the effect of the Dark Matter should be minimal. As such, we believe our "minimal" model of the distribution of the normal matter of the Galaxy adopted above is good enough for the purpose of illustrating the general nature of effects arising from a self-consistent description of the Galaxy's phase space structure that includes the mutual gravitational interaction of the visible matter and the Dark Matter components of the Galaxy. The formalism of this paper and the numerical procedure adopted by us are, however, quite general and applicable to any given model of the mass distribution of the Galaxy.

In our numerical calculations, we have taken the DM density at the solar location, $\rho_{\mathrm{DM},\odot} = \rho_{\mathrm{DM}}(R = R_0, 0)$, as the "observable" density parameter of the King model instead of the parameter ρ_1 in equation (14). We have run a large number of numerical models of the Galaxy for three different values of $\rho_{\mathrm{DM},\odot} = 0.2\,, 0.3$ and $0.4\ \mathrm{GeV/\,cm^3}$, in each case with a wide range of values of the other two King model parameters r_t and σ and with the visible matter parameters fixed as described above, to determine the parameters that best describe the Galaxy's rotation curve data mentioned above.

B. Dark Matter Density Profile

The main effect of the gravitational influence of the visible matter on the DM halo, namely, increased central concentration and reduced core radius of the DM density profile, is illustrated in Figure 1. The left panel of Figure 1 shows

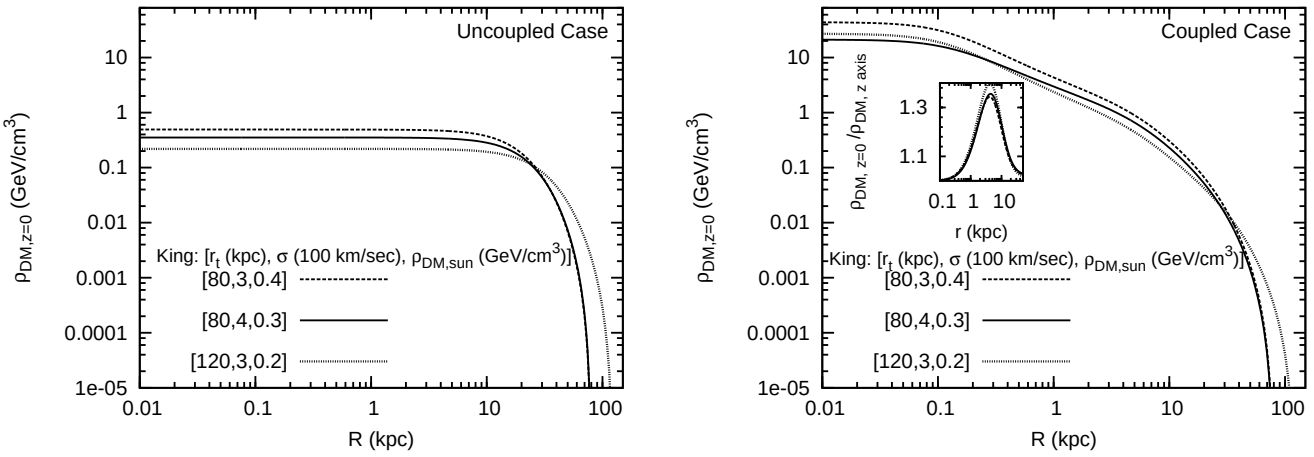

FIG. 1: The density profiles of the lowered (truncated) isothermal dark matter halo described by the King model DF, eq. (4), (a) in absence ("uncoupled"), and (b) in presence ("coupled"), of the visible matter described by equations (18) and (19), for three different sets of values of the King model parameters $(r_t, \sigma, \rho_{\mathrm{DM},\odot})$ that yield good fits (in the coupled case) to the rotation curve data of the Galaxy up to $\sim 60\,\mathrm{kpc}$. In (b) the density profiles refer to those on the equatorial plane ($z = 0$) of the Galaxy. The inset in (b) shows the ratio of the density on the $z = 0$ plane to that on the z axis as a function of galactocentric distance in the coupled case, for the same chosen sets of the King model parameters as indicated.

the density profiles of a 'pure' spherically symmetric finite-size DM halo described by the King model DF (4) without including the gravitational influence of the visible matter on the DM (hereafter referred to as the "uncoupled" case), whereas the right panel shows the DM density profiles (in the plane of the Galactic disk ($z = 0$)) under the additional gravitational influence of the visible matter (hereafter referred to as the "coupled" case). The curves in both panels are for three different sets of values of the King model parameters $(r_t, \sigma, \rho_{\mathrm{DM},\odot})$ as indicated, that yield good fits (in the coupled case) to the rotation curve data of the Galaxy up to $\sim 60\,\mathrm{kpc}$ (see discussions below and Figure 2). The increased central density and the reduced core size of the density profiles in the coupled case relative to those in the uncoupled case are clearly seen.

Another direct effect of the gravitational influence of the visible matter on the DM is the enhancement of the DM density on the plane of the Galactic disk ($z = 0$) relative to that off the disk. The inset in the right panel of Figure 1 shows this effect clearly where it is seen that this disk enhancement of DM density can be as large as ~ 30 – 40 %.

The typical scale length of this "dark matter disk" is a few kpc.

C. Rotation Curves

Figure 2 shows our theoretically calculated rotation curves for the Galaxy with its DM halo described by the King

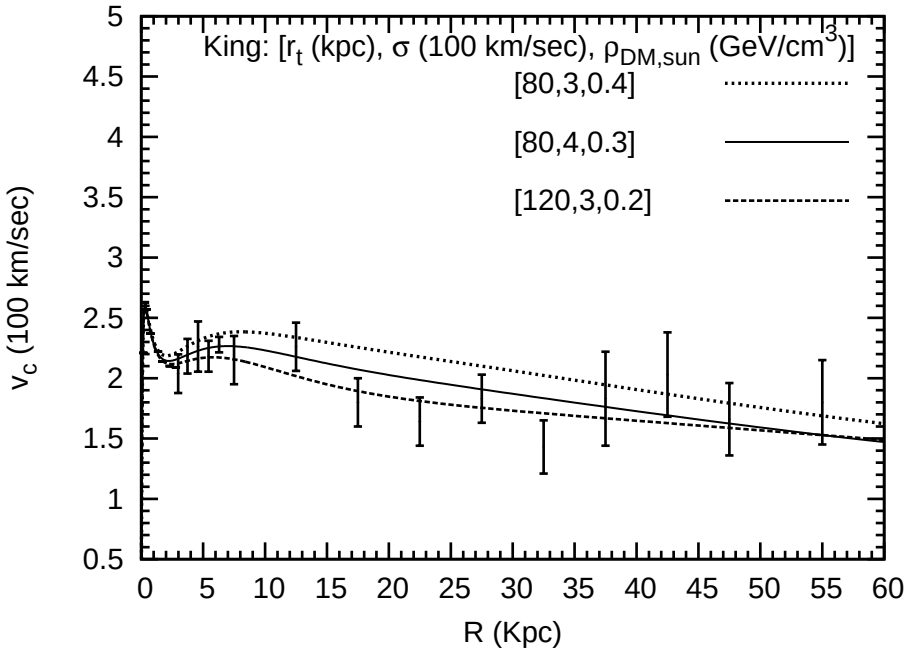

FIG. 2: Rotation curves for the Galaxy with its DM halo described by the King model DF, eq. (4) and including the gravitational effect of the visible matter described by equations (18) and (19), for three different sets of values of the King model parameters $(r_t\,, \sigma\,, \rho_{\rm DM,\odot})$ as indicated. The curves are shown for three different values of $\rho_{\rm DM,\odot}$, and in each case, the curve shown corresponds to the values of the other two parameters (r_t and σ) that yield best fit to the rotation curve data of the Galaxy estimated in Ref. [29]. The data with error bars are from Table 3 of Ref. [29] (their data set $V_{\rm cir,II}$ corresponding to their simulation II) for galactocentric distances $R \geq 7.5\,$kpc, and from Ref. [34] for $R < 7.5\,$kpc.

model DF, eq. (4) and including the gravitational effect of the visible matter described by equations (18) and (19), for three different sets of values of the King model parameters $(r_t, \sigma, \rho_{\rm DM,\odot})$ as indicated. For comparison, the rotation curve data for R up to 55 kpc given, for $R \geq 7.5\,$kpc, in Table 3 of Ref. [29] (their data set $V_{\rm cir,II}$ corresponding to their simulation II) are shown together with the data from Ref. [34] for $R < 7.5\,$kpc. The theoretical rotation curves are shown for $\rho_{\rm DM,\odot} = 0.2\,, 0.3$ and $0.4\,{\rm GeV/\,cm^3}$, and in each case, the shown theoretical curve corresponds to the values of the other two parameters (r_t and σ) that yield best fit (giving lowest χ^2) to the above mentioned rotation curve data of the Galaxy.

For the range of King model density parameter considered ($0.2 \leq \rho_{\rm DM,\odot} \leq 0.4\,{\rm GeV/\,cm^3}$), the "global" best fit to the rotation curve data (giving globally lowest value of χ^2) is obtained for the King model DM parameter values $\rho_{\rm DM,\odot} = 0.2\,{\rm GeV/\,cm^3}$, $r_t \simeq 120\,$kpc and $\sigma \simeq 300\,{\rm km\,s^{-1}}$ (the dashed curve in Figure 2) [5]. The separate contributions of the visible matter (VM) and the Dark Matter (DM) components to the total rotation curve and the total mass of the Galaxy for this "best-fit" set of parameter values are shown in Figure 3.

It is of interest to note that the DM halo mass for the best-fit model obtained above, $M_{\rm DM} \sim 1.3 \times 10^{11}\,M_\odot$, is only marginally more than the total visible matter mass, $M_{\rm VM} \sim 8.4 \times 10^{10}\,M_\odot$, giving a total Galaxy mass of

[5] Note that, as already mentioned, the parameter σ in the King model is not to be confused with the one-dimensional velocity dispersion of the DM particles.

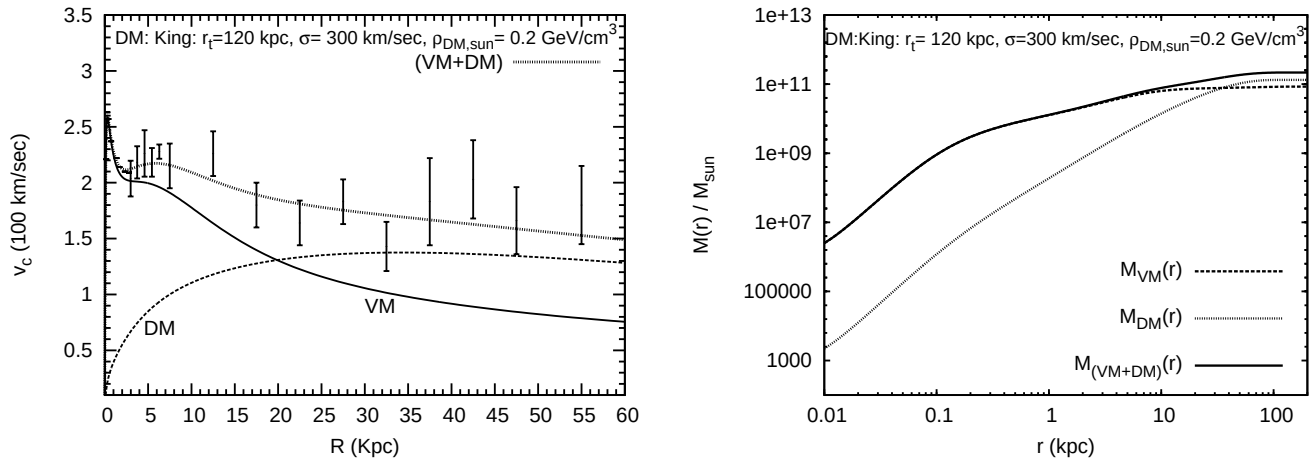

FIG. 3: The contributions of the visible matter (VM) and the dark matter (DM) components to (a) the total rotation curve (left panel) and (b) total mass (right panel) of the Galaxy for the best-fit King model DM halo parameters $\rho_{\rm DM,\odot} = 0.2\,{\rm GeV/\,cm^3}$, $r_t = 120\,{\rm kpc}$ and $\sigma \simeq 300\,{\rm km\,s^{-1}}$. The rotation curve data in the left panel are the same as in Figure 2.

$\sim 2.1 \times 10^{11}\, M_\odot$ for the adopted VM model. Actually, this is fairly independent of the exact values of the VM model parameters adopted as long as those parameters are such that the VM by itself gives the dominant contribution to the rotation curve data at small $R \ll R_\odot$. The main reason for the relatively low DM halo mass is the declining nature of the rotation curve beyond the solar circle. Within the context of the truncated isothermal models of the DM halo described by the King models studied here, higher DM halo mass models — which can be obtained by choosing larger values of one or more of the parameters $\rho_{\rm DM,\odot}$, r_t or σ than those of the best-fit model obtained above — typically lead to rising or non-declining rotation curves beyond the solar circle, and are thus unable to explain the declining rotation curve data.

D. Maximum Speed and Speed Distribution of the particles

The self-consistently calculated maximum speeds of DM particles in the halo as a function of R are shown in Figure 4 (left panel) for the same three sets of King model halo parameters as in Figure 2. The corresponding normalized speed distribution functions of the DM particles (in the Galactic rest frame), $f(v) \equiv \frac{4\pi v^2}{\rho(\mathbf{x})} f(\mathbf{x},\mathbf{v})$ (with $\int f(v) dv = 1$), at Sun's location ($R = R_\odot$, $z = 0$), are also shown (right panel). For comparison, the Maxwellian speed distribution for the Standard Halo Model (SHM) at sun's location is also shown. Evidently, the speed distribution for the truncated "isothermal" halo is significantly non-Maxwellian, especially at the high speed end of the distribution, not unlike the behavior found in recent numerical simulations [25].

For the three King model parameter sets considered in the left panel of Figure 4 the maximum speeds of the DM particles at the location of Sun are, from bottom to top, 396, 403 and 439 km/s, respectively. These values and the speed distribution functions shown in Figure 4 will be used below in the calculation of the expected WIMP detection rates and analysis of the results of the direct detection experiments. We emphasize that the above values refer to the maximum speeds that a *dark matter particle* can have at the location of the Sun. Since stars in the Galaxy do not in general follow the same velocity distribution function as the dark matter particles, they can have speeds larger than the maximum speeds of the dark matter particles mentioned above. Stars with speeds larger than the escape speeds determined by the total mass and radius of the halo (see equation (11)), will, of course, eventually escape from the Galaxy.

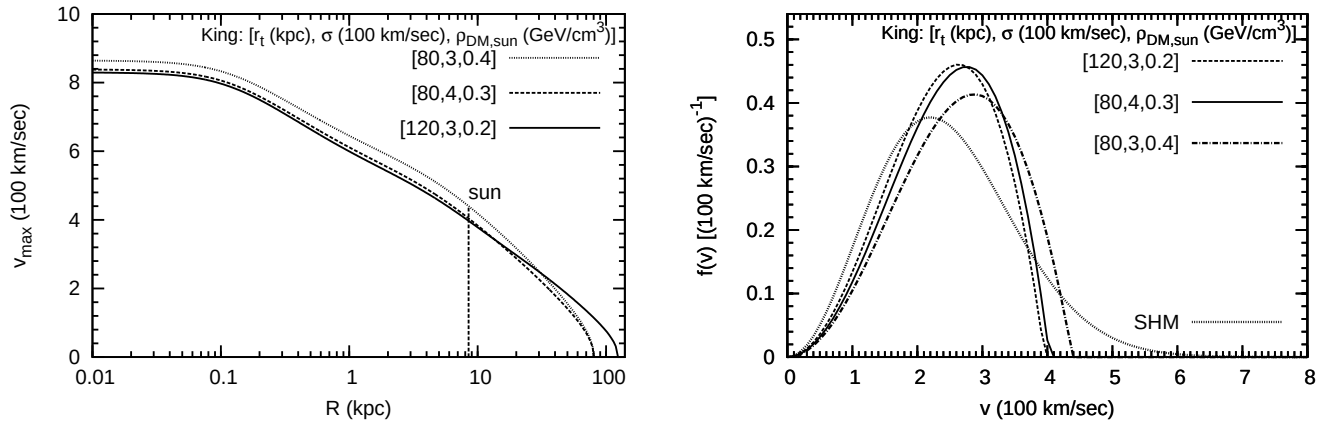

FIG. 4: Maximum speed $v_{\rm max}(\mathbf{x}) = \sqrt{2\Psi(\mathbf{x})}$ in the Galactic equatorial plane as a function of Galactocentric distance R (left panel) and the normalized speed ($v = |\mathbf{v}|$) distribution function of the DM particles, $f(v) \equiv \frac{4\pi v^2}{\rho(\mathbf{x})} f(\mathbf{x}, \mathbf{v})$ (right panel), at Sun's location ($R = R_\odot$, $z = 0$), for the same three sets of King model parameters as in Figure 2 as well as for the Maxwellian speed distribution in the case of Standard Halo Model (SHM).

III. IMPLICATIONS OF THE SELF-CONSISTENT TRUNCATED ISOTHERMAL HALO MODEL FOR THE ANALYSIS OF WIMP DIRECT DETECTION EXPERIMENTS

A. Direct Detection of WIMPs: The Basic Formalism

For simplicity we restrict our attention in this paper to the case of elastic scattering of the WIMPs from nuclei. Consider a WIMP (hereafter denoted by χ) of mass m_χ scattering elastically from a nucleus of mass M. The nucleus receives a recoil energy, $E_R = q^2/(2M) = (\mu^2 u^2/M)(1 - \cos\theta^*)$, where θ^* is the scattering angle in the centre of momentum frame, q the momentum transferred to the recoiling nucleus, $\mu = m_\chi M/(m_\chi + M)$ is the WIMP-nucleus reduced mass and $u = |\mathbf{u}|$ is the speed of the WIMP relative to the nucleus assumed to be at rest on earth. The minimum WIMP speed that can produce a recoil energy E_R of the nucleus is

$$u_{\rm min}(E_R) = \left(\frac{ME_R}{2\mu^2}\right)^{1/2} . \tag{20}$$

The differential event rate per unit detector mass (typically measured in counts/day/kg/keV) can be written as [2, 8]

$$\frac{d\mathcal{R}}{dE_R}(E_R, t) = \frac{\sigma(q)}{2m_\chi \mu^2} \rho_\chi \xi(E_R, t) \,, \tag{21}$$

where $\rho_\chi \equiv \rho_{\rm DM,\odot}$ is the density of WIMPs in the solar neighborhood, $\sigma(q)$ is the WIMP-nucleus effective interaction cross section, and

$$\xi(E_R, t) = \int_{u > u_{\rm min}(E_R)} d^3\mathbf{u} \frac{\tilde{f}(\mathbf{u}, t)}{u} \,. \tag{22}$$

Here $\tilde{f}(\mathbf{u}, t)$ is the time-dependent velocity distribution of the WIMPs in the solar neighborhood *relative to the detector at rest on earth*, and $u_{\rm min}$ is defined in equation (20). Recall that $f_{\rm K}(\mathbf{x}, \mathbf{v})$ defined in equation (4) refers to the rest frame of the Galaxy, and has no explicit dependence on time. The time dependence of $\tilde{f}$ arises from the motion of the earth with respect to the Galactic rest frame. The two distribution functions are simply related as

$$\tilde{f}(\mathbf{u}, t) = \frac{1}{\rho_\chi} f_{\rm K} \left(\mathbf{x} = \mathbf{x}_\odot, \mathbf{v} = \mathbf{u} + \mathbf{v}_{\rm E}(t)\right) \,, \tag{23}$$

where $\mathbf{x}_\odot$ represents the sun's position ($R = 8.5\,{\rm kpc}, z = 0$) and $\mathbf{v}_{\rm E}(t)$ is the earth's velocity vector *in the Galaxy's rest frame*. Note that the DF $f_{\rm K}$ vanishes for speed $v \geq v_{\rm max}$ defined in equation (9).

Using equation (23) we can explicitly write equation (22) as

$$\xi(E_R,t)=\frac{2\pi}{\rho_{\rm DM,\odot}}\int_{-1}^{1}d(\cos\theta)\;\Theta\left(u_{\rm max}-u_{\rm min}\right)\int_{u_{\rm min}(E_R)}^{u_{\rm max}(\cos\theta)}u f_{\rm K}\left(\mathbf{x}=\mathbf{x}_\odot,\mathbf{v}=\mathbf{u}+\mathbf{v}_{\rm E}(t)\right)du\,, \tag{24}$$

where $u_{\rm max}$ is the positive root of the equation

$$v_{\rm max}^2=u_{\rm max}^2+v_{\rm E}^2+2u_{\rm max}v_{\rm E}\cos\theta\,, \tag{25}$$

with $v_{\rm max}$ given by equation (9) evaluated at $\mathbf{x}=\mathbf{x}_\odot$, and $v_{\rm E}=|\mathbf{v}_{\rm E}|$ given by [18]

$$v_{\rm E}(t)=\;v_\odot+v_{\rm E,orb}\cos\gamma\cos\left[\omega(t-t_0)\right]\;, \tag{26}$$

where $v_\odot\approx v_{c,\odot}+12\,{\rm km\,s^{-1}}$ is the magnitude of the dominant component of sun's total velocity vector (which includes its circular velocity around the Galaxy of magnitude $v_{c,\odot}\approx 220\,{\rm km\,s^{-1}}$ and its "peculiar" velocity of magnitude $\approx 12\,{\rm km\,s^{-1}}$) in the Galactic rest frame, $v_{\rm E,orb}\approx 30\,{\rm km\,s^{-1}}$ is the average orbital speed of the earth around the sun, $\cos\gamma\approx 0.51$, $\omega=2\pi/365$ and $t_0=152.5$ (corresponding to 2nd June when the earth's speed with respect to the Galactic rest frame is maximum), t being counted in days. It is the periodic variation of $v_{\rm E}$, equation (26), that gives rise to the annual modulation signal claimed to have been detected by the DAMA collaboration.

For detectors composed of more than one kind of elements, the total differential event (i.e., nuclear recoil) rate is

$$\left(\frac{d\mathcal{R}}{dE_R}\right)_{\rm tot}=\sum_i f_i\left(\frac{d\mathcal{R}}{dE_R}\right)_i\,, \tag{27}$$

where f_i is the mass fraction of, and $\left(\frac{d\mathcal{R}}{dE_R}\right)_i$ the differential event rate (eq. (21)) for, the nuclear species i, with corresponding nuclear mass M_i, WIMP-nucleus cross section $\sigma_i(q)$ and WIMP-nucleus reduced mass μ_i.

The number of nuclear recoil events in a recoil energy range between E_R^1 and E_R^2 is

$$N_R(E_R^1,E_R^2)=\sum_i\int_{E_R^1}^{E_R^2}dE_R\,\left(\frac{d\mathcal{R}}{dE_R}\right)_i\mathcal{K}_i(E_R)\,, \tag{28}$$

where $\mathcal{K}_i=\mathcal{M}_iT\epsilon(E_R)$ is the total exposure of the detector, $\mathcal{M}_i$ being the total mass of the species i in the detector, T the total exposure time, and $\epsilon(E_R)$ the energy-dependent detector efficiency.

The WIMP-nucleus total effective scattering cross section, $\sigma(q)$, can be written as a sum of two contributions arising from spin-independent (SI) and spin-dependent (SD) effective couplings of the WIMP to the detector nucleus [2, 8, 19] :

$$\sigma(q)=\sigma_{\rm SI}(q)+\sigma_{\rm SD}(q)\,. \tag{29}$$

Spin-independent (SI) (or *Coherent*) Scattering : In this case, it is assumed that the WIMP interacts coherently with the nucleus as a whole. The cross section is generally written as [2]

$$\sigma(q)=\sigma_0|F(q)|^2 \tag{30}$$

where σ_0 is the zero-momentum WIMP-nucleus scattering cross section, and $F(q)$ is a momentum dependent form factor that arises from the finite size of the nucleus. The form factor $F(q)$ is normalized to $F(0)=1$. The coherent nature of the interaction is implemented under the usual assumption that σ_0 scales with the square of the atomic mass number A (number of protons plus neutrons) of the nucleus. For purely scalar interactions, with equal WIMP couplings to protons and neutrons, one can write σ_0 in terms of the WIMP-proton (or WIMP-neutron) effective cross section $\sigma_{\chi p}=\sigma_{\chi n}$ as

$$\sigma_0^{\rm SI}=\sigma_{\chi p}^{\rm SI}\left(\frac{\mu}{\mu_{\chi p}}\right)^2A^2\,, \tag{31}$$

where $\mu_{\chi p}$ is the WIMP - proton reduced mass.

We shall use the conventional Helm form of the nuclear form factor [2, 8, 19] :

$$F(q) = 3e^{-q^2 s^2/2\hbar^2}\, \frac{\sin(qr_0/\hbar) - (qr_0/\hbar)\cos(qr_0/\hbar)}{(qr_0/\hbar)^3}\,, \tag{32}$$

with $s = 0.9\,\mathrm{fm}$, the nuclear skin thickness and $r_0 = 1.14A^{1/3}$ fm, the effective nuclear radius.

Spin-dependent (SD) Scattering : In this case the WIMP couples to the total spin J of the nucleus which has contributions from the spins of the individual protons and neutrons within the nucleus. Following Ref. [19] we use the effective WIMP-nucleus SD cross section generically written in the form [35]

$$\sigma_{\rm SD}(q) = \frac{32\mu^2 G_F^2}{2J+1}\left[a_p^2 S_{pp}(q) + a_p a_n S_{pn}(q) + a_n^2 S_{nn}(q)\right]\,, \tag{33}$$

where a_p and a_n are respectively the axial four-fermion WIMP-proton and WIMP-neutron couplings in units of $2\sqrt{2}G_F$ [36–38]. The nuclear structure functions $S_{pp}(q)$, $S_{nn}(q)$ and $S_{pn}(q)$ are taken, for Ge from Ref. [39], for Si from Ref. [40], for Al from Ref. [41], and for Na, I and Xe from Ref. [42].

In this paper, following the standard practice, we shall study the situations when either $a_n = 0$ or $a_p = 0$; the relevant effective cross section in the two cases will be denoted by $\sigma^{\rm SD}_{\chi p}$ and $\sigma^{\rm SD}_{\chi n}$, respectively. In general both a_n and a_p can be non-zero, but we will not consider this case here.

B. Results of Direct Detection Experiments and Analysis Techniques

To illustrate the general implications of our halo model for the WIMP mass and cross section as implied by the results of direct-detection experiments, we consider in this paper the results of three of the "null" experiments (i.e., those without any definite claim of detection so far), namely, CDMS-II [11, 43], CRESST [12] and XENON10 [13, 14], in addition to those of the DAMA collaboration [10] which has claimed a positive signal based on the claimed detection of the annual modulation of the recoil event rate. As we shall see, results of these three null experiments together provide useful information regarding the question of compatibility of the positive results of DAMA with the negative results of other experiments over a wide range of the WIMP mass m_χ from ~ 1 GeV to 100 GeV. Below, we first describe the DAMA results and the analysis procedure we follow in order to derive the constraints on WIMP mass and interaction cross section imposed by the results, and then discuss the same for the null experiments.

DAMA/NaI and DAMA/LIBRA :
The DAMA collaboration [9, 10] has claimed detecting a non-zero annual modulation signal at a confidence level (C.L) of 8.2σ in their number of detected nuclear recoil events over a period of seven (for the DAMA/NaI experiment [9]), plus four (for the DAMA/LIBRA experiment [10]), annual cycles, with a total exposure of 0.82 ton-year[6]. The DAMA collaboration attributes this annual modulation to the periodic variation of $v_{\rm E}$, equation (26), which results in a periodic variation of the recoil event rate (see discussions in the previous subsection).

Given the time dependence of $v_{\rm E}$, equation (26), the time dependence of the differential event rate (21) due to motion of the earth around the sun can be approximately written as [6, 7, 19]

$$\frac{d\mathcal{R}}{dE_R}(E_R, t) \approx S_0(E_R) + S_m(E_R)\cos\omega(t - t_0)\,, \tag{34}$$

where S_0 is the average recoil rate over a year and S_m is the "modulation amplitude" defined as

$$S_m(E_R) = \frac{1}{2}\left[\frac{d\mathcal{R}}{dE_R}\,(E_R,\,\mathrm{June2}) - \frac{d\mathcal{R}}{dE_R}\,(E_R,\,\mathrm{Dec2})\right]\,. \tag{35}$$

---

[6] While this paper was being prepared, the DAMA/LIBRA collaboration released their latest results with an additional exposure of 0.34 ton-year corresponding to two additional annual cycles [44]. With this, the statistical significance of the annual modulation signal is now 8.9σ for the cumulative exposure. We do not include these new results in this paper.

A nonzero value of S_m is taken to be a signal for WIMP-induced recoils.

To compare with DAMA data given in specific recoil energy bins, the average value of S_m over a given energy range is calculated as:

$$S_m^{E_1-E_2} = \frac{1}{E_2 - E_1} \int_{E_1}^{E_2} S_m(E_R) dE_R \,. \tag{36}$$

A scintillation detector such as that used in the DAMA experiment directly detects only the part of the recoil nucleus energy that goes into electromagnetic channel and produces the observed scintillation. The actual energy of the recoil nucleus E_R is related to the detectable energy from the scintillation light yield, E_D — often called the "electron-equivalent (ee) energy" and denoted by "keVee" with energy in units of keV — through the relation $E_D = QE_R$, where the "quenching factor" $Q(< 1)$ depends on the nuclear material composing the scintillation detector. For the DAMA detector (composed of NaI crystal), $Q_{\rm Na} \approx 0.3$ and $Q_{\rm I} \approx 0.09$. At the same time, as first pointed out in Ref. [45] and studied in detail in the context of the DAMA detector in Ref. [46], for certain energies and incidence angles of the particle (for example, along the crystal axis), the incident particle transfers energy only to the electrons (rather than to the nuclei) of the scintillator material. In such a case, called "channeling", one has $Q \approx 1$. We shall use the following simple parametrizations, suggested in Ref. [47], of the fractions of "channeled" events for recoiling Sodium and Iodine nuclei, based on simulation results given in Ref. [46] for the DAMA experiment:

$$f_{\rm Na} \simeq \frac{1}{1 + 1.14 E_R(\,{\rm keV})} \,, \quad f_{\rm I} \simeq \frac{1}{1 + 0.75 E_R(\,{\rm keV})} \,. \tag{37}$$

Note that the use of keVee is only a bookkeeping device to distinguish the actually measured energy by the detector from the true recoil energy, the actual energy *unit* still being keV. For detectors for which the concept of channeling does not exist (for example, CDMS or XENON), the quenching factor can be included in the energy calibration and final data quoted directly in terms of the recoil energy.

For the analysis of the DAMA results, in this paper we consider for simplicity only the 2-bin data set given by the DAMA collaboration [10], namely, the low-energy bin 2 – 6 keVee within which a non-zero modulation amplitude is measured, and the high energy bin 6 – 14 keVee in which the modulation amplitude is consistent with zero. Table I gives the modulation amplitudes (S_m) measured by DAMA in these two energy bins.

Energy (keVee)	Modulation Amplitude (S_m) (counts/day/kg/keVee)
2 – 6	0.0131 ± 0.0016
6 – 14	0.0009 ± 0.0011

TABLE I: DAMA modulation amplitude data [10]

The efficiency of the DAMA detector is taken to be unity. To compare with the actual experimental data we take into account the finite energy resolution of the detector whereby the actually measured energies are taken to be normally distributed about the true detectable energy E_D (i.e., the energy that would be measured if the detector had 100% energy resolution) with a standard deviation [48] $\sigma(E_D) = (0.448\,{\rm keV})\sqrt{E_D/\,{\rm keV}} + 0.0091 E_D$. Thus, the expected modulation amplitude is obtained by convolving equation (35) (after changing the integration variable to $E_D = QE_R$) with a normalized Gaussian with the above standard deviation. The expected modulation amplitude over a given interval of measured energy between E_{D1} and E_{D2} is then calculated from equation (36) after the above convolution.

With the theoretically expected modulation amplitude in the k-th energy bin, $S_{m,k}^{\rm th}$, calculated as described above, we perform, following the simple analysis procedure of Ref. [18], a χ^2 fit to the experimental modulation amplitude data given in Table I with

$$\chi^2 \equiv \sum_k \left(\frac{S_{m,k} - S_{m,k}^{\rm th}}{\sigma_k} \right)^2 \,, \tag{38}$$

where $S_{m,k}$ is the experimentally measured modulation amplitude in the k-th energy bin and σ_k the corresponding error in the experimental value given in Table I. In this simple analysis procedure, there are only two free parameters in the problem, namely, the WIMP mass m_χ and the relevant WIMP-nucleon cross section σ_χ. The latter is $\sigma^{\rm SI}_{\chi p}$ in the SI case (see eq. (31)), and either $\sigma^{\rm SD}_{\chi p}$ or $\sigma^{\rm SD}_{\chi n}$ in the SD case (see eq. (33) and the discussions following it). For a given value of m_χ we find $\chi^2_{\rm min}$, the minimum value of χ^2, by scanning over the values of the relevant cross section σ_χ. The 90% C.L. allowed region of the relevant cross section, for the given value of m_χ, is then found by accepting those values of σ_χ for which $\chi^2 - \chi^2_{\rm min} \leq 2.71$, provided $\chi^2_{\rm min} < 2$. More rigorous multi-parameter analysis procedures described, for instance, in Ref. [19], may alter the constraints derived here at some quantitative level. However, we believe the simple analysis procedure adopted here is sufficient for our main purpose of illustrating, in the context of our self-consistent model of the dark halo of the Galaxy, the general nature of the constraints in the (m_χ, σ_χ) parameter space implied by the experimental results. The resulting constraints imposed by the DAMA results are described in the next subsection together with those imposed by the null results of the other experiments.

Experiments giving null results :
Table II summarizes the relevant features of the "null" experiments we consider in this analysis. Details of each experiment can be found in the cited References.

Experiment	Target	Effective exposure (kg-days)	Threshold (keV)
CDMS-II [11]	Ge	304.5 (SI), 23.5 (SD)	10
CDMS-II [43]	Si	12.1 (SI), 0.57 (SD)	7
CRESST-I [12]	Al_2O_3	1.51 (SI), 0.53 (SD)	0.6
XENON10 [13, 14]	Xe	136 (SI), 64.7 (SD)	6.1

TABLE II: Relevant features of the experiments with null results considered in this paper.

For the purpose of analysis, the null experiments can be divided into two classes: (a) Those which report no events at all (after all the relevant cuts are employed), and (b) those which report events (after analysis cuts) but ascribe them to background. In both cases, we follow the simple analysis procedure outlined in Ref. [18]. For the former case (a), we derive 90% C.L. upper limit on the relevant WIMP cross section σ_χ for a given WIMP mass m_χ by using Poisson statistics and demanding that the theoretically predicted number of events, N, over the entire energy range of interest be such as to allow a Poisson probability of observing zero events as bad as 10% but not worse. This corresponds to $N(m_\chi, \sigma_\chi) = 2.3$. In the case (b), a simplified version of Yellin's [49] optimum interval method, as suggested in Ref. [18], is used, whereby we again calculate, for a given mass m_χ, and for all contiguous combination of energy bins, the 90% C.L. upper limit allowed theoretically expected number of events $N(m_\chi, \sigma_\chi)$ corresponding to the observed number of events n as dictated by Poisson statistics, i.e., by the formula $\sum_{j=0}^{j=n} \frac{N^j}{j!} \exp(-N) = 0.1$, and choose the most stringent (i.e., the lowest) upper limit value of σ_χ so obtained.

CDMS-II (Ge) [11] :
This is currently the experiment with the largest effective exposure amongst all currently running experiments. Two events were observed, after applying all cuts, in the signal region at recoil energies 12.3 keV and 15.5 keV in the 10 – 100 keV window. The effective quenching factor is already included in the energy calibration. Since the estimated probability of observing 2 or more background events in this window is $\sim 23\%$, these events were ascribed to background. We obtain upper limits on the relevant WIMP cross section as a function of WIMP mass using the simplified version of Yellin's [49] optimum interval method described above. In this analysis we have used a minimum bin width of 0.4 keV. The total effective exposure used in this calculation includes the spectrum-averaged equivalent exposure of ≈ 194.1 kg-days (for a WIMP mass of $\sim 60\,{\rm GeV}/c^2$) reported in Ref. [11] combined with that of CDMS-II collaboration's previous published paper [50], ~ 110.4 kg-days (after reduction of the figure quoted in Ref. [50] by a factor of $\sim 9\%$ due to improved estimate of their detector mass as prescribed in Ref. [11]). The above figures include the approximately constant (in energy) detector efficiency of $\sim 30\%$ already folded in.

For spin-dependent interaction, only the ^{73}Ge isotope, whose natural abundance is $\approx 7.73\%$, is sensitive to the WIMPs. The effective exposure for SD interaction is correspondingly reduced and is significantly less than that for the SI interaction case.

CDMS-II (Si) [43] :
This experiment employs a high purity silicon crystal as the detector material. No events passed all the data analysis cuts. We derive 90% C.L. upper limit on the relevant cross section as a function of the WIMP mass by using Poisson statistics discussed above, i.e., by demanding that, for a given WIMP mass m_χ, the upper limit value of cross section yield 2.3 events.

For SD interactions, only the ^{29}Si isotope, whose natural abundance is 4.68%, is effective.

CRESST-I [12] :
The Phase I of the CRESST experiment employed sapphire (Al_2O_3) detectors with an exposure of 1.51 kg-days over an energy range of 0.6-20 keV. Measured energies are calibrated to recoil energy ($Q = 1$). All the observed events were ascribed to background. We take into account the energy resolution of the detector described by a Gaussian distribution of the measured energies around the true value with a standard deviation $\sigma(E_R) = \sqrt{(0.220\,\mathrm{keV})^2 + (0.017 E_R)^2)}$ [12][7]. Upper limits were obtained similar to CDMS-II(Ge) analysis with a smallest allowed energy-interval width of 1.2 keV [12].

For SD case only the Aluminum is sensitive since Oxygen has J=0.

XENON10 [13, 14] :
XENON10 is a dual phase (liquid and gas) xenon time projection chamber and uses the ratio of ionization to scintillation yield for discriminating between the dominant electron-recoil background and the looked for nuclear-recoil WIMP signal over a nuclear-recoil energy range of $\sim$ 6.1–36.5 keV ($Q = 1$) with the relevant energy calibration parameter $\mathcal{L}_{\mathrm{eff}} = 0.14$ [19]. We use an energy resolution of $\sigma(E_R) = (0.579\,\mathrm{keV})\sqrt{E_R/\,\mathrm{keV}} + 0.021 E_R$ as suggested in Ref. [19]. A total of 10 events (without background subtraction) were recorded in the WIMP signal region for a total effective exposure of about 136 kg-days after analysis cuts. As in the case of the CDMS-II Ge analysis described above, we again obtain upper limits on the relevant WIMP cross section as a function of WIMP mass using the simplified version of Yellin's optimum interval method described above.

For spin-dependent WIMP interaction, only the isotopes ^{129}Xe (spin-1/2) with a natural abundance of $\sim$ 26.4% and ^{131}Xe (spin-3/2) with a natural abundance of $\sim$ 21.2% are effective.

C. Implications for the WIMP parameters : Exclusion plots and compatability of null results with DAMA signal

Figures 5 – 7 show our main results in terms of the constraints on the relevant WIMP-nucleon cross sections as a function of the WIMP mass, as implied by the results of the direct detection experiments. In all these Figures, the regions above the curves are excluded at the 90% C.L. by the results of the respective experiments.

Figure 5 shows our 90% C.L. upper limits on WIMP-nucleon spin-independent cross section as a function of WIMP mass as implied by the latest CDMS-II results [11]. For our halo model with $\rho_{\mathrm{DM},\odot} = 0.3\,\mathrm{GeV/\,cm^3}$ (with other halo parameters fixed by fitting to the rotation curve data), the lowest upper limit on the WIMP-nucleon spin-independent cross section is $3.4 \times 10^{-8}\,\mathrm{pb}$ at $m_\chi = 69\,\mathrm{GeV}$ — coincidentally almost identical to the value of $3.8 \times 10^{-8}\,\mathrm{pb}$ quoted in Ref. [11] which uses SHM in their analysis (presumably with a chosen value of the Galactic escape speed of $600\,\mathrm{km\,s^{-1}}$ [8]). However, for our self-consistent halo model that gives the best fit to the new rotation curve data — this model has $\rho_{\mathrm{DM},\odot} = 0.2\,\mathrm{GeV/\,cm^3}$ — the above upper limit on the SI cross section changes to $\sim 5.3 \times 10^{-8}\,\mathrm{pb}$ at $m_\chi = 71\,\mathrm{GeV}$. The upper limit value of the cross section approximately scales inversely with the value of $\rho_{\mathrm{DM},\odot}$.

Figures 6 and 7 show the results of our study of the compatibility of the DAMA experiment's claimed positive result (based on their original 2-bin annual modulation amplitude data) with the null results of various other experiments, for the cases of WIMP-nucleon spin-independent and spin-dependent cross sections, respectively. For the spin-independent

[7] Ref. [12] actually quotes their energy resolution in terms of the FWHM, $\Delta {E_R}^{\mathrm{FWHM}}$, which is related to the standard deviation σ by $\Delta {E_R}^{\mathrm{FWHM}} \approx 2.354\sigma$.

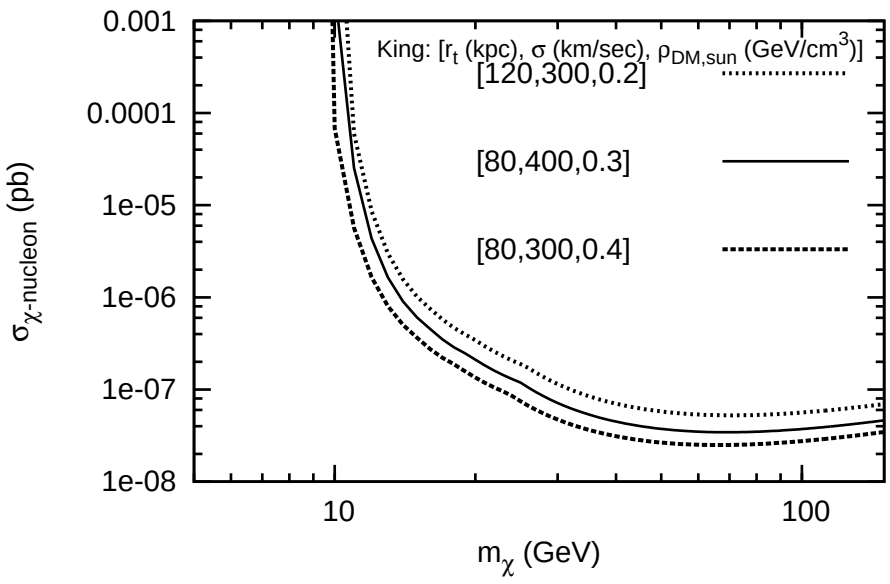

FIG. 5: 90% C.L. upper limits on the WIMP-nucleon spin-independent cross section as a function of WIMP mass as implied by the latest CDMS results [11], for our self-consistent truncated isothermal (King) model of Milky Way's DM halo described by the same three sets of King model parameters as in Figure 2. The WIMP speed distribution function and the maximum WIMP speeds for these King model parameters used in deriving the above upper limits are as shown in Figure 4.

case, we find that there is a range of small WIMP masses, $2.6 \lesssim m_\chi \lesssim 10.8\,\mathrm{GeV}$, within which DAMA's claimed modulation signal is consistent with the null results of other experiments. The allowed WIMP-nucleon SI cross section varies from $\sim 1.0 \times 10^{-2}\,\mathrm{pb}$ at the lower end of the WIMP mass range to $\sim 1.2 \times 10^{-5}\,\mathrm{pb}$ at the upper mass end. For the spin-dependent case, the DAMA-compatible mass range for WIMP-neutron interaction (i.e., $a_p = 0$) is $2.5 \lesssim m_\chi \lesssim 7.4\,\mathrm{GeV}$, with the corresponding WIMP-neutron interaction cross section range of 9.5×10^3 – 42.0 pb. For the case of WIMP-proton interaction (with $a_n = 0$), the corresponding WIMP mass and cross section ranges are $2.3 \lesssim m_\chi \lesssim 16\,\mathrm{GeV}$ and 79.0 – 0.45 pb, respectively.

We emphasize that the DAMA-compatible ranges of WIMP mass and cross sections obtained above are based on our simple analysis procedure using the original 2-bin DAMA annual modulation amplitude data, and are comparable to those obtained earlier within the context of the SHM, e.g., in Ref. [19] (their 2-bin analysis results). More rigorous analyses using DAMA bins over smaller intervals, as done, e.g., in [19], should be able to place more restrictive constraints on the DAMA-compatible ranges of WIMP mass and cross section within the context of our halo model. This will be taken up in a work now in progress.

IV. SUMMARY AND CONCLUSIONS

The standard halo model (SHM) of the dark matter halo of the Galaxy, customarily used in the analysis of the results of WIMP direct detection experiments, is not suitable for describing a finite-size system such as the Galaxy. In the SHM, the DM halo of the Galaxy is described as an isothermal sphere with a Maxwellian velocity distribution of its constituent particles. The isothermal sphere solution of the steady-state collisionless Boltzmann equation is actually infinite in extent and has a divergent total mass with the mass contained inside a radius r increasing linearly with r [20]. In the literature on direct detection of WIMP dark matter particles, it is a common practice to truncate the Maxwellian speed distribution assumed in the SHM at a chosen value of the local escape speed of the Galaxy. This, however, is not a self-consistent procedure because the resulting truncated speed distribution does not in general satisfy the steady-state collisionless Boltzmann equation which a system of collisionless particles such as WIMPs should. Moreover, the results of analysis of the outcome of a direct detection experiment would depend on the value of the escape speed chosen, which is quite uncertain (see, e.g., Ref. [51]).

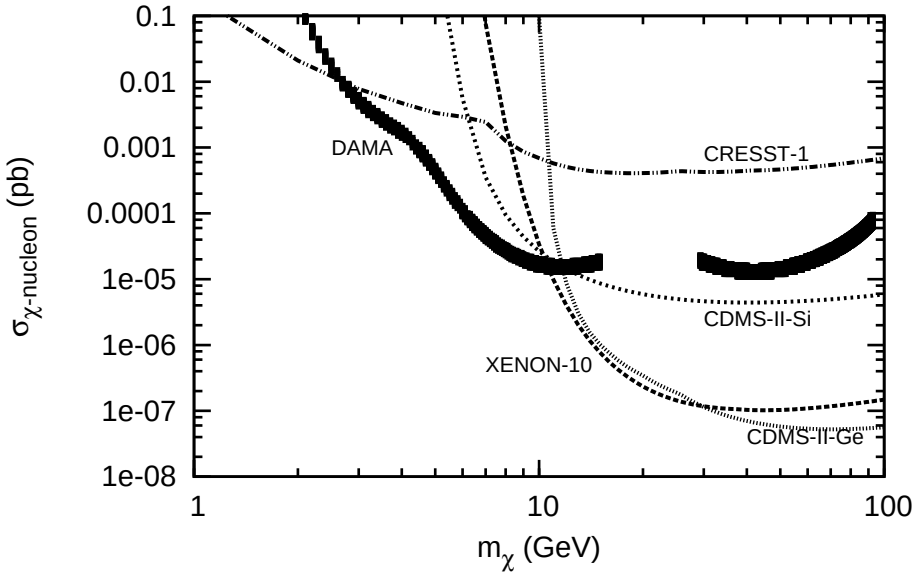

FIG. 6: 90% C.L. allowed region in the WIMP mass vs. WIMP-nucleon spin-independent cross section plane implied by the DAMA modulation signal, for our best-fit halo model with parameters $r_t = 120\,\mathrm{kpc}$, $\sigma = 300\,\mathrm{km\,s^{-1}}$ and $\rho_{\mathrm{DM},\odot} = 0.2\,\mathrm{GeV/\,cm^3}$. Also shown are 90% C.L. upper limits on cross section as a function of WIMP mass as implied by the null results of other experiments, as indicated, again for the same King model halo parameters.

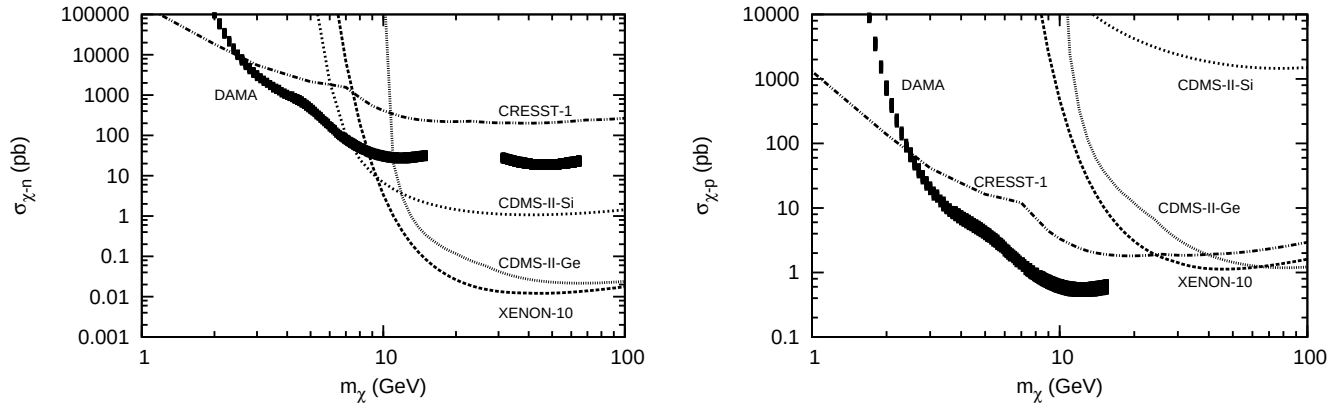

FIG. 7: 90% C.L. allowed region in the WIMP mass vs. WIMP-neutron ($a_p = 0$) (left panel) and WIMP-proton ($a_n = 0$) (right panel) spin-dependent cross section plane implied by the DAMA modulation signal, for our self-consistent truncated isothermal (King) model of Milky Way's DM halo with parameters $r_t = 120\,\mathrm{kpc}$, $\sigma = 300\,\mathrm{km\,s^{-1}}$ and $\rho_{\mathrm{DM},\odot} = 0.2\,\mathrm{GeV/\,cm^3}$. Also shown are 90% C.L. upper limits on the cross sections as a function of WIMP mass as implied by the null results of other experiments, again for the same King model halo parameters.

In this paper we have presented a self-consistent model of the finite-size dark halo of the Galaxy with its phase space distribution function described by a truncated isothermal model ("King" model). We have also included the gravitational influence of the observed visible matter on the structure of the DM halo in a self-consistent manner. In this model the velocity distribution function of the WIMPs constituting the halo is non-Maxwellian, with a cut-off at a maximum velocity that is self-consistently determined by the model itself. We have determined the parameters of our halo model by a fit to a recently determined circular rotation curve of the Galaxy that extends up to a Galactocentric

distance of $\sim 60\,\mathrm{kpc}$ [29]. A noticeable feature of this rotation curve is that it declines with the Galactocentric radius beyond $\sim 10\,\mathrm{kpc}$. This imposes strong constraints on the (truncation) radius, density and mass of the DM halo and hence on the total mass of the Galaxy. Specifically, for values of local DM density in the range $\rho_{\mathrm{DM},\odot} = 0.2$ – $0.4\,\mathrm{GeV/\,cm^3}$, reasonable fits to the rotation curve data require the truncation radius of the halo to be in the corresponding range $r_t \approx 120$ – 80 kpc, in all cases restricting the total mass of the Galaxy (including its DM halo) to relatively low values of $M_{\mathrm{Galaxy}} \lesssim 3 \times 10^{11}\,M_\odot$. Note, however, that the rotation curve estimated in Ref. [29], which is used in determining the parameters of our halo model, was derived assuming a value of $\approx 220\,\mathrm{km\,s^{-1}}$ for the local standard of rest. On the other hand, as suggested in Ref. [26], the value of the local standard of rest may have to be revised upward to a value of $v_{c,\odot} \approx 250\,\mathrm{km\,s^{-1}}$. This would require appropriate scaling up of the rotation curve data of Ref. [29], which in turn will require an appropriately higher value of $\rho_{\mathrm{DM},\odot}$ and a correspondingly higher value of the total mass of the Galaxy.

Interestingly, we find that the upper limits on the relevant WIMP-nucleon interaction cross section implied by the null results of the direct detection experiments are primarily determined by the chosen value of the local DM density $\rho_{\mathrm{DM},\odot}$ — scaling roughly inversely with the value of $\rho_{\mathrm{DM},\odot}$ — and are relatively less sensitive to the other parameters of the model such as the truncation radius and total mass of the halo. For our best-fit self-consistent lowered isothermal halo model with parameter values $\rho_{\mathrm{DM},\odot} = 0.2\,\mathrm{GeV/\,cm^3}$ and $r_t = 120\,\mathrm{kpc}$, that provides the best fit to the rotation curve data of Ref. [29], the null result of the CDMS-II experiment [11], for example, gives a 90% C.L. upper limit on the WIMP-nucleon spin-independent (SI) interaction cross section of $\sim 5.3 \times 10^{-8}\,\mathrm{pb}$ at a WIMP mass of 71 GeV.

Concerning the issue of the compatability of the claimed positive signal reported by the DAMA collaboration with the null results from the other experiments, we find, within the context of a simple analysis procedure using the original 2-bin DAMA annual modulation data, that there exist regions of the WIMP mass vs. WIMP-nucleon cross section with small WIMP masses typically in the range ~ 2 – 16 GeV, within which the DAMA's claimed annual modulation signal is consistent with the null results of other experiments. While this strengthens the possibility of a low mass WIMP as a DM candidate — a possibility also indicated by several earlier analyses done using the SHM — a more rigorous analysis using DAMA bins over smaller intervals must be performed before a more definitive conclusion can be reached in this regard. Very recently, the CoGeNT collaboration [52] has also reported an excess of low (nuclear recoil) energy events, which may also be pointing towards a low-mass WIMP DM candidate. We shall discuss these issues within the context of our self-consistent model of the Galaxy's dark halo in a work now in progress.

Acknowledgments

We thank Susmita Kundu for discussions.

Bibliography

[1] WMAP collaboration, N. Jarosik et al., arXiv:1001.4744.
[2] G. Jungman, M. Kamionkowski and K. Griest, Phys. Rep. **267** (1996) 195 [arXiv:hep-ph/9506380].
[3] G. Bertone, D. Hooper and J. Silk, Phys. Rep. **405** (2005) 279.
[4] D. Hooper and S. Profumo, Phys. Rep. **453** (2007) 29.
[5] M.W. Goodman and E. Witten, Phys. Rev. **D 31** (1985) 3059.
[6] A.K. Drukier, K. Freese and D.N. Spergel, Phys. Rev. **D 33** (1986) 3495.
[7] K. Freese, J.A. Frieman and A. Gould, Phys. Rev. **D 37** (1988) 3388.
[8] J.D. Lewin and R.F. Smith, Astropart. Phys. **6** (1996) 87.
[9] R. Bernabei et al., Riv. Nuovo Cim. **26N1** (2003) 1 [arXiv:astro-ph/0307403].
[10] DAMA collaboration, R. Bernabei et al., Eur. Phys. J. **C 56** (2008) 333 [arXiv:0804.2741].
[11] CDMS collaboration, Z. Ahmed et al., Science **327** (2010) 1619; Z. Ahmed et al., arXiv:0912.3592.
[12] G. Angloher et al., Astropart. Phys. **18** (2002) 43.
[13] XENON collaboration, J. Angle et al., Phys. Rev. Lett. **100** (2008) 021303 [arXiv:0706.0039].
[14] XENON collaboration, J. Angle et al., Phys. Rev. Lett. **101** (2008) 091301 [arXiv:0805.2939].
[15] COUPP collaboration, E. Behnke et al., Science **319** (2008) 933 (2008) [arXiv:0804.2886].
[16] PICASSO collaboration, S. Archambault et al., Phys. Lett. **B 682** (2009) 185.
[17] A. Bottino, F. Donato, N. Fornengo and S. Scopel, Phys. Rev. **D 78** (2008) 083520 [arXiv:0806.4099]; S. Chang, G. D. Kribs, D. Tucker-Smith and N. Weiner, Phys. Rev. **D 79** (2009) 043513 [arXiv:0807.2250]; S. Chang, A. Pierce and N. Weiner, Phys. Rev. **D 79** (2009) 115011 [arXiv:0808.0196]; M. Fairbairn and T. Schwetz, JCAP **09** (2009) 037 [arXiv:0808.0704];

D. Hooper, F. Petriello, K. M. Zurek and M. Kamionkowski, Phys. Rev. **D 79** (2009) 015010 [arXiv:0808.2464]; S. Andreas, T. Hambye and M. H. G. Tytgat, JCAP **10** (2008) 034 [arXiv:0808.0255].
[18] F.J. Petriello and K.M. Zurek, JHEP **09** (2008) 047 [arXiv:0806.3989].
[19] C. Savage, G. Gelmini, P. Gondolo and K. Freese, JCAP **04** (2009) 010 [arXiv:0808.3607].
[20] J. Binney and S. Tremaine, Galactic Dynamics, 2nd Edition (Princeton University Press, Princeton, 2008).
[21] D. Lynden-Bell, MNRAS **136** (1967) 101.
[22] J.H. Oort, Bull. Astr. Inst. Netherlands **6** (1937) 249; ibid. **15** (1960) 45.
[23] N. Bahcall, Astrophys. J. **276** (1984) 169.
[24] P. Salucci, F. Nesti, G. Gentile and C.F. Martins, arXiv:1003.3101.
[25] F.S. Ling, E. Nezri, E. Athanassoula and R. Teyssier, arXiv:0909.2028.
[26] M.J. Reid et al., Astrophys. J **700** (2009) 137 [arXiv:0902.3913].
[27] R. Cowsik, C. Ratnam and P. Bhattacharjee, Phys. Rev. Lett. **76** (1996) 3886; *ibid* **78** (1997) 2262.
[28] R. Cowsik, C. Ratnam, P. Bhattacharjee and S. Majumdar, New Astron. **12** (2007) 507 [arXiv:astro-ph/0703262].
[29] X.X. Xue et al., Astrophys. J. **684** (2008) 1143 (2008).
[30] J.K. Adelman-McCarthy et al., Astrophys. J. Suppl. **175** (2008) 297.
[31] A.M. Green, Phys. Rev. **D 66** (2002) 083003 [arXiv:astro-ph/0207366].
[32] J. Caldwell and J. Ostriker, Astrophys. J. **251** (1981) 61; K. Kuijken and G. Gilmore, MNRAS **239** (1989) 571; ibid. **239** (1989) 605; ibid. **239** (1989) 651; Astrophys. J. **L9** (1991) 367.
[33] T. Naab and J. Ostriker, MNRAS **366** (2006) 899.
[34] M. Honma and Y. Sofue, PASJ **49** (1997) 453.
[35] J. Engel, Phys. Lett. **B 264** (1991) 114. (1991).
[36] P. Gondolo in *XXXI Rencontres de Moriond: Dark Matter in Cosmology, Quantum Measurements, Experimental Gravitation*, Les Arcs, France, 1996 [arXiv:hep-ph/9605290].
[37] D.R. Tovey et al., Phys. Lett. **B 488** (2000) 17 [arXiv:hep-ph/0005041].
[38] P. Gondolo et al., JCAP **07** (2004) 008 [arXiv:astro-ph/0406204].
[39] V. Dimitrov, J. Engel and S. Pittel, Phys. Rev. **D 51** (1995) 291 [arXiv:hep-ph/9408246].
[40] M.T. Ressell et al., Phys. Rev. **D 48** (1993) 5519.
[41] J. Engel, M. T. Ressell, I. S. Towner and W. E. Ormand, Phys. Rev. **C 52** (1995) 2216 [arXiv:hep-ph/9504322].
[42] M.T. Ressell and D.J. Dean, Phys. Rev. **C 56** (1997) 535 [arXiv:hep-ph/9702290].
[43] CDMS collaboration, D.S. Akerib et al., Phys. Rev. Lett. **96** (2006) 011302 [arXiv:astro-ph/0509259].
[44] DAMA collaboration, R. Bernabei et al., arXiv:1002.1028.
[45] E.M. Drobyshevski, Mod. Phys. Lett. **A 23** (2008) 3077 [arXiv:0706.3095].
[46] DAMA collaboration, R. Bernabei et al., Eur. Phys. J. **C 53** (2008) 205 [arXiv:0710.0288].
[47] R. Foot, Phys. Rev. **D 78** (2008) 043529 [arXiv:0804.4518].
[48] DAMA collaboration, R. Bernabei et al., Nucl. Instrum. Meth. **A 592** (2008) 297 [arXiv:0804.2738].
[49] S. Yellin, Phys. Rev. **D 66** (2002) 032005 [physics/0203002].
[50] CDMS collaboration, Z. Ahmed et al., Phys. Rev. Lett. **102** (2009) 011301 [arXiv:0802.3530].
[51] M.C. Smith et al, MNRAS **379** (2007) 755 [arXiv:astro-ph/0611671].
[52] CoGeNT collaboration, C.E. Aalseth et al, arXiv:1002.4703.